Faraday Discussions

Crystal Melting and Vitrification Behaviors of the Three-Dimensional Nitrile-Based Metal–Organic Framework

Journal:	*Faraday Discussions*
Manuscript ID	FD-ART-01-2020-000003.R1
Article Type:	Paper
Date Submitted by the Author:	31-Jan-2020
Complete List of Authors:	Das, Chinmoy; Kyoto University, Institute for Integrated Cell-Material Sciences Horike, Satoshi; Kyoto University, Institute for Integrated Cell-Material Sciences

Crystal Melting and Vitrification Behaviors of the Three-Dimensional Nitrile-Based Metal–Organic Framework

Chinmoy Das[1] and Satoshi Horike*[1,2,3,4]

[1] AIST-Kyoto University Chemical Energy Materials Open Innovation Laboratory (ChEM-OIL), National Institute of Advanced Industrial Science and Technology (AIST), Yoshida-Honmachi, Sakyo-ku, Kyoto 606-8501, Japan

[2] Institute for Integrated Cell-Material Sciences, Institute for Advanced Study, Kyoto University, Yoshida-Honmachi, Sakyo-ku, Kyoto 606-8501, Japan

[3] Department of Synthetic Chemistry and Biological Chemistry, Graduate School of Engineering, Kyoto University, Katsura, Nishikyo-ku, Kyoto 615-8510, Japan

[4] Department of Materials Science and Engineering, School of Molecular Science and Engineering, Vidyasirimedhi Institute of Science and Technology, Rayong 21210, Thailand

Abstract

A three-dimensional (3D) metal–organic framework $[Ag(pL_2)(CF_3SO_3)]\cdot 2C_6H_6$ (*p*L2 = 1,3,5-tris(4-ethynylbenzonitrile)benzene), composed of Ag^+ and tripodal nitrile ligands, was prepared to enable the investigation of its crystal melting and vitrification behaviors. The guest-free state showed a crystal melting at 271 °C, and the liquid state transformed into a glassy state via cooling. The vitrification of the crystalline compound into an amorphous glassy state was also obtained by mechanical hand-grinding. The structure of the glassy state retained the 3D networked structure, confirmed by FT-IR, X-ray absorption, and scattering measurements. The mechanically induced glass showed a small uptake of CO_2 and a strong affinity for benzene and H_2O vapors, confirmed

by gas sorption isotherms. Studies on powder X-ray diffraction have revealed that a vitrified structure returns to the original 3D crystalline structure by exposure to these vapors.

Introduction

Metal–organic frameworks (MOFs) and coordination polymers (CPs) have been extensively studied for the designability of their crystal structures and fruitful functionalities. In the past few years, the crystal melting and formation of the glassy state of MOFs/CPs have been highlighted.[1-4] Their non-crystalline properties offer unique functions, such as optical properties, fast and selective gas/ion transport, and hybridization with other substances for catalysis and sensing.[5-8] Their moldable characters and phase transition properties are also attractive adhesive or switching materials.[9, 10] The ligand system of melting/vitrifying MOFs/CPs has been limited. Some representatives are metal azolates [M = Zn^{2+}, Co^{2+}: zeolitic imidazolate framework (ZIF)-4, ZIF-62, etc.][2, 11] and metal azolate phosphates (M = Zn^{2+}, Cd^{2+}, Cr^{2+}, Mn^{2+}).[1, 5, 6, 12, 13] For crystalline MOFs/CPs, other ligand systems such as carboxylate, pyridyl, quinoid, phosphonate, and amine have been powerful platforms for constructing extended structures.[14-19] As we have discovered in the crystalline state, the ligand library should expand toward melting/vitrifying MOFs/CPs alongside the azolates.

A useful ligand system for constructing two-dimensional (2D) or three-dimensional (3D) frameworks includes cyanide and nitrile. Traces of Prussian blue analogs or Hofmann clathrates are evident in history, and many crystal structures with nitrile-based organic ligands have been identified to date.[20-22] The coordination bond between the nitrile group and the metal ion is also known to be labile and dynamic. Negative thermal expansion and structural flexibility by external stimuli are examples of the dynamic feature of nitrile-based MOFs/CPs.[23-27] The labile nature of nitrile would be useful to construct melting/vitrifying structures. Hence, in this paper, we focus on a 3D MOF $[Ag(pL_2)(CF_3SO_3)]\cdot 2C_6H_6$ (1-a, *p*L2 = 1,3,5-tris(4-ethynylbenzonitrile)benzene) whose crystal structure was reported in 1995.[28] We used differential scanning calorimetry (DSC) and Fourier-transform infrared spectroscopy (FT-IR) to investigate the crystal melting and vitrification of this compound; we also used X-ray absorption (XAS) and X-ray total scattering to study the structure of a glassy state. Knowing that a glassy state consists of 3D coordination

networks, we also conducted gas/vapor adsorption studies to check permanent porosity and examine the process of glass-to-crystal transformation.

Experimental

Materials and instruments

All chemicals and solvents used in the syntheses were of reagent grade and used without further purification. $AgCF_3SO_3$ (Silver triflate, 98%) was purchased from Tokyo Chemicals Industry Co., Ltd. and super dehydrated benzene (99.5%) was purchased from Wako Pure Chemical Industries, Ltd.

Synthesis of [Ag(*p*L2)(CF_3SO_3)]·$2C_6H_6$ (1-a): The synthesis procedure was modified from the literature report.[28] [Ag(*p*L2)(CF_3SO_3)]·$2C_6H_6$ (1-a, *p*L2 = 1,3,5-tris(4-ethynylbenzonitrile)benzene) was synthesized by solvothermal method with a temperature controller oven. $AgCF_3SO_3$ and *p*L2 were transferred into an Ar-filled glovebox. $AgCF_3SO_3$ (149 mg, 0.58 mmol) and *p*L2 (59 mg, 0.13 mmol) were separately dissolved into 4 mL and 10 mL of super dehydrated benzene, respectively. Both the solutions were stirred separately for 10 mins in Ar atmosphere for complete dissolution. A white suspension was immediately formed when these two solutions were mixed together. The turbid solution was transferred into a Teflon lined autoclave and it was fixed inside a stainless steel vessel. It was kept inside the temperature controller oven and heated at 120 °C for 4 h. It was slowly cooled down to 28 °C with a rate of 1.9 °C h^{-1} over the period of 48 h. Needle shaped crystals were isolated after the reaction. Crystals were washed with benzene for 3 times and dried in ambient condition (98 mg).

Preparation of 1: 1-a was degassed under vacuum at 120 °C for 6 h to obtain 1.

Preparation of 1-MIG: 1-MIG was prepared by hand-grinding the microcrystals of 1 in agate mortar under Ar atmosphere for 30 minutes.

Powder X-ray diffraction (PXRD): PXRD patterns were collected on a Rigaku MiniFlex with CuKα anode (wavelength λ = 1.5418 Å) ranging from 2θ value of 3 to 50° with a step of 0.02°, and the speed of the data collection is 5° min^{-1}.

Fourier transform infrared spectroscopy (FT-IR): FT-IR spectra were collected using a Bruker Optics ALPHA FT-IR spectrometer with Universal ATR accessory under Ar, and a Nicolet ID5 ATR under air operating at ambient temperature between 4000 to 500 cm^{-1}.
Thermogravimetric analysis (TGA): TGA-DTA profiles were collected using a Rigaku Thermo plus TG 8120 (N_2) and TG 8121 (Ar) apparatus in the temperature range of 30 °C to 500 °C at a heating rate of 10 °C min^{-1}.
Differential scanning calorimetry (DSC): The differential scanning calorimetry (DSC) was carried out with Hitachi High-Tech Science Corporation model DSC7020 at the heating rate of 10 °C min^{-1} under the N_2 atmosphere. A real-time camera is equipped with the instrument for sample observation and automatic capturing of the photograph at an interval of 2 °C min^{-1}. The melting point and glass transition temperature were determined by using a software TA7000 Standard Analysis (Ver. 5.0).
Gas and solvent sorption isotherms: CO_2 adsorption isotherms were collected using BELSORP-mini at −78.15 °C. Benzene and water adsorption isotherms were collected using BELSORP-aqua at 25 °C. Solvents were pre-dried and freeze-pump-thaw was carried out three times to enhance purity of the degassed solvent.
X-ray total scattering: The powder sample of 1 and 1-MIG was sealed in a quartz glass capillary (ϕ = 2 mm) inside Ar-filled glovebox. The X-ray total scattering data were collected at 25 °C with four CdTe and two Ge detectors covering the Q range up to 25 $Å^{-1}$ at the BL04B2 beamline at the Super Photon Ring (SPring-8, Hyogo, Japan). The incident beam was monochromated at $\lambda = 0.2020$ Å. G(r) is obtained from the Fourier transformation of $S(Q)$ with a Lorch modification function through Igor Pro software.[29]

X-ray absorption spectroscopy (XAS): The samples were prepared by mixing with appropriate amounts of boron nitride (BN) and pressed into pellet of 10 mm diameter. X-ray absorption spectra were collected at the Aichi Synchrotron Radiation Center (Aichi SR) on beamline BL11S2. The data was processed using the IFEFFIT library.[30] Fourier transformation was k^3-weighted in the k range from 3-14 $Å^{-1}$. Ag foil internal energy calibration was measured simultaneously with each sample. The energy was defined by assigning the first inflection point of the Ag foil spectrum to 25516 eV.

Results and Discussion

Structural description

Solvothermal reaction was used to synthesize a 3D CP $[Ag(pL2)(CF_3SO_3)]\cdot 2C_6H_6$ (1-a, *p*L2 = 1,3,5-tris(4-ethynylbenzonitrile)benzene) (Fig. 1A). An asymmetric unit of 1-a consists of each two Ag^+, *p*L2 and $CF_3SO_3^-$, with one being coordinated to Ag^+ and the other retaining a counter anion with disorder. Two benzene molecules were also present in the cavity. Four coordination numbers at each Ag^+ was satisfied by three –C≡N groups from three different *p*L2 and one $CF_3SO_3^-$, creating a distorted trigonal pyramidal geometry. Additionally, three coordination numbers in another Ag^+ satisfied by three –C≡N groups of three *p*L2 created a trigonal planar geometry. The bridging of each *p*L2 to Ag^+ forms an interpenetrated structure of 3D networks, and the assembled structure provides honeycomb architecture (Fig. 1B). We confirmed the structure of as-synthesized 1-a by the powder X-ray diffraction (PXRD) pattern, which matched the simulated pattern of the single-crystal X-ray structure reported in the literature (Fig. 1C).[28]

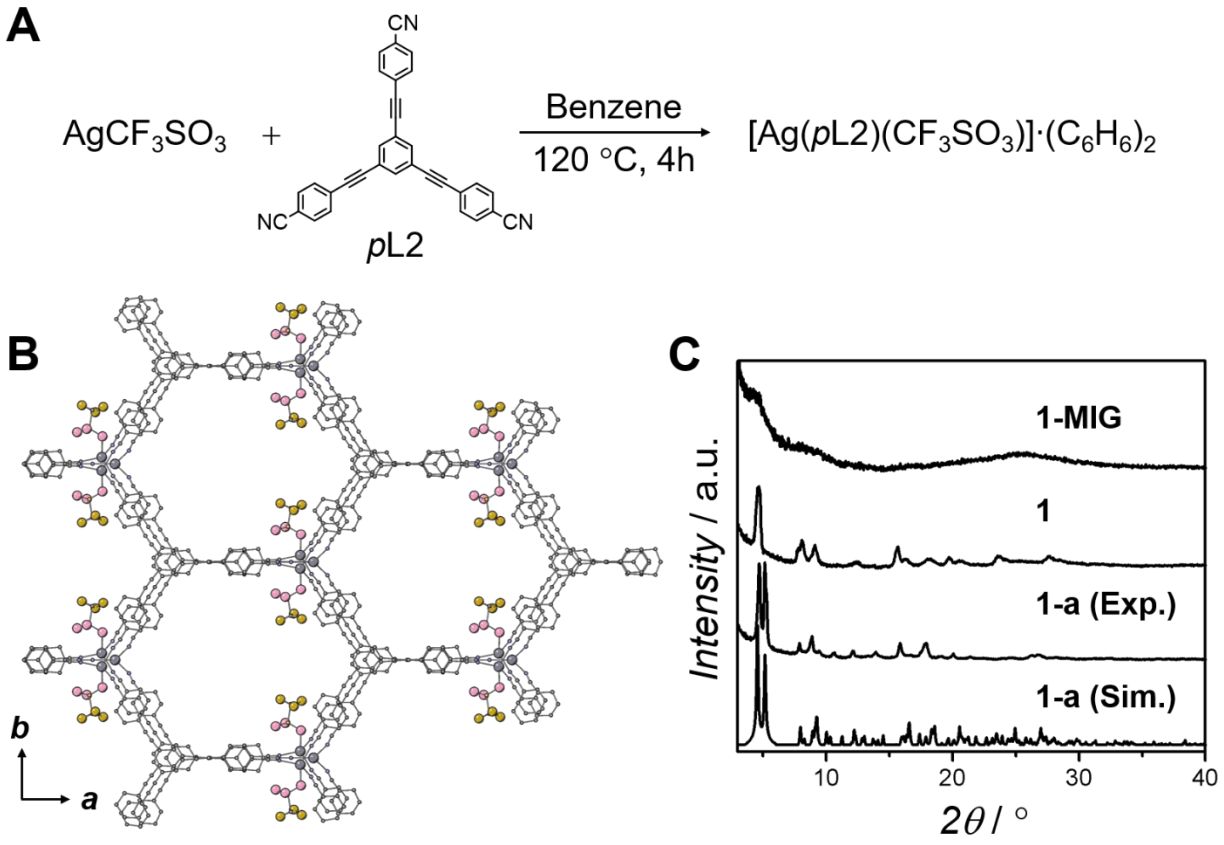

Fig. 1. (A) Synthesis scheme of $[Ag(pL2)(CF_3SO_3)]\cdot 2C_6H_6$ (1-a). (B) Structural illustration of 1-a. Gray: C, blue: N, pink: O, yellow: S, ocher: F, gray (large): Ag. Hydrogen and guest benzene molecules and $CF_3SO_3^-$ are omitted for clarity. (C) PXRD patterns of 1-a with a simulated pattern from single-crystal X-ray structure, 1 and 1-MIG at room temperature.

Structural characterization and thermal behaviors of 1-a and 1

Thermogravimetric analysis (TGA) of 1-a (Fig. 2A) showed that a gradual weight loss from 25 °C to 120 °C corresponds to the removal of benzene molecules from the structure. No weight loss was observed from 125 °C to 280 °C. According to the TGA profile, 1-a was degassed under vacuum at 120 °C for 6 h to obtain guest-free state 1. PXRD pattern of 1 (Fig. 1C) was different from 1-a; this suggests that the structure of 1 changes by degas treatment. We did not succeed in solving the crystal structure of 1. To learn whether 1 retains the CP (networked) structure, we carried out elemental analysis, FT-IR, variable temperature (VT)-PXRD, and X-ray

absorption measurements. The elemental analysis results show that 1 matches guest-benzene-free [Ag(*p*L2)(CF_3SO_3)]. FT-IR (Fig. 2B) yielded a −C≡N stretching vibration band, which appeared at 2248 cm^{-1} for 1-a of all the *p*L2 bridges of Ag^+ ions. −C≡N stretching vibration band of *p*L2 itself was 2228 cm^{-1}, which confirms that the coordination of *p*L2 to Ag^+ makes 20 cm^{-1} of high wavelength shift. FT-IR of 1 shows the identical stretching band position of 1-a (2248 cm^{-1}), suggesting that coordination bonds between Ag^+ and *p*L2 are preserved to form 3D structures.[31, 32]

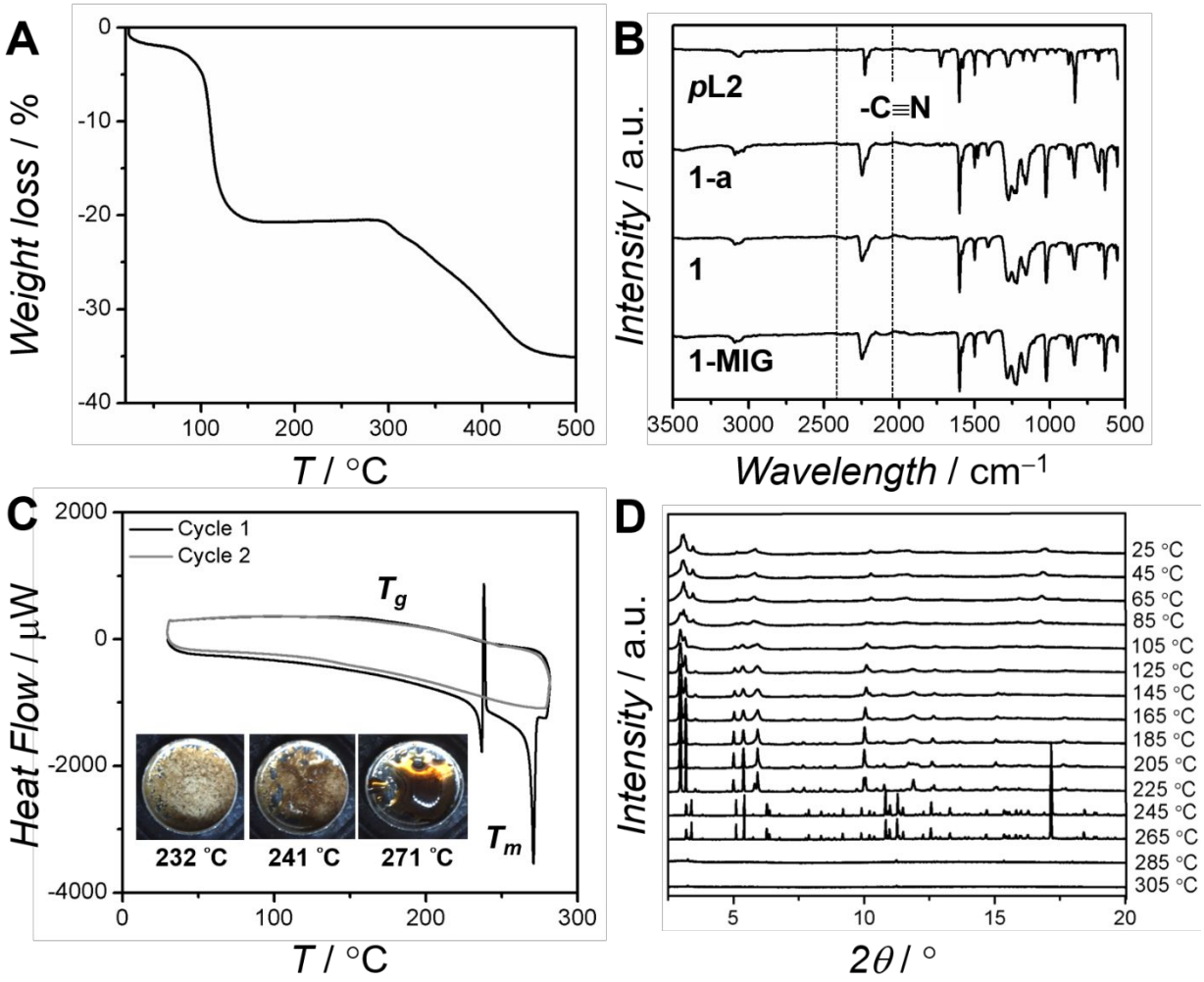

Fig. 2. (A) TGA profile for 1-a. The scan rate is 10 °C min^{-1}. (B) FT-IR spectra of *p*L2, 1-a, 1, and 1-MIG. −C≡N stretching vibration bands are highlighted with dotted lines. (C) Two cycles of heating and cooling processes of DSC profiles of 1. *In situ* snapshots of 1 in the first heating process are also shown. T_m represents the melting temperature, and the ramping

rate is 10 K min^{-1}. (D) VT-PXRD patterns from 25 °C to 305 °C of 1-a, collected under the Ar atmosphere. Wavelength λ = 0.999338(2) Å.

X-ray absorption spectroscopy (XAS) were performed for 1-a and 1 to understand the local atomic and electronic structure around Ag^{+}.[33, 34] X-ray absorption near-edge structure (XANES) spectra (Fig. 3A) confirmed that core-shell 1s to 5p electronic transition at 25516 eV for both 1-a and 1.[35] We treated 1-a as a reference sample which maintain its oxidation state of +1 in the crystal structure. The superposed spectra of XANES for 1-a and 1 suggests the same electronic structure in 1 as like 1-a. Fourier transformed Ag *K*-edge extended X-ray absorption fine structure (EXAFS) profiles (Fig. 3B) show that the scattering pathways for two main components are identified in RDFs, located at 1.3-2.1 Å and 2.2-3.2 Å. The scattering pathways of Ag-O/Ag-N and other neighboring atoms fall in the similar RDFs for both 1-a and 1. These XAS studies also support the view that 1 preserves the 3D structures with the same coordination geometries of Ag^{+} as like 1-a.

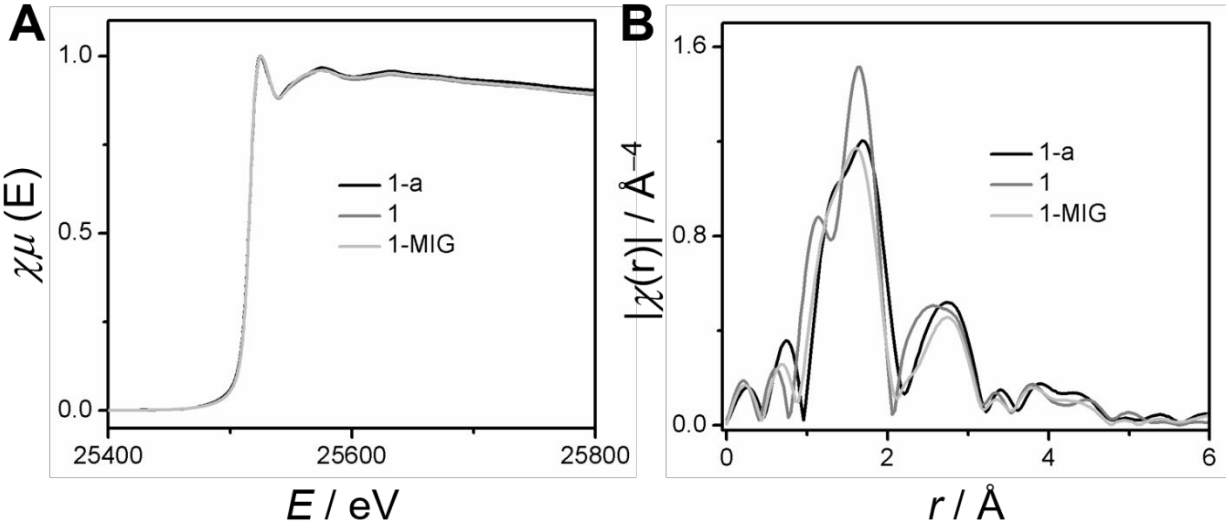

Fig. 3. (A) XANES and (B) Ag *K*-edge EXAFS spectra of 1-a, 1, and 1-MIG at room temperature.

We measured DSC for 1 in the N_2 atmosphere (Fig. 2C). It exhibited two peaks at 237 °C and 271 °C. We also collected images of sample upon first heating, which suggests that the first peak

at 237 °C is a solid-to-solid phase transition mainly because powder morphology does not change significantly. The peak at 271 °C represents crystal melting, with clear morphological change at that temperature. In the process of melting, the color of 1 changed from pale yellow to dark brown. We did not observe any peak in the cooling process but found a glass transition temperature (T_g) at 161 °C. We also carried out second heating and cooling measurements of DSC; however, we found it hard to distinguish T_g and T_m. To confirm these structural changes upon heating, we measured the VT-PXRD of 1-a (Fig. 2D). Between 25 °C and 225 °C, the peaks remained unchanged, although each peak became sharper because of an improvement in crystallinity with guest release and a slight shift to the lower angle arising from the thermal expansion. We found a drastic change in patterns from 225 °C to 245 °C. This change corresponds to the peak at 237 °C in DSC; thus, we conclude that this is a solid-to-solid structural change. Further heating from 265 °C to 285 °C made all peaks disappear mainly because of crystal melting. As a result of DSC and PXRD, 1 shows a crystal melting at 271 °C and that the liquid state transfers to the glassy state by gentle cooling to room temperature.

Structural characterization and thermal behaviors of 1-MIG

Mechanical milling can be used to fabricate the glassy state of MOFs/CPs directly from their crystalline state.[5, 13, 36, 37] This mechanical method will make it unnecessary to process the vitrification through the melt state. We conducted hand-grinding of 1 inside the Ar-filled glove box to prepare 1-mechanically induced glass (1-MIG). This is an amorphous structure confirmed by PXRD (Fig. 1C). It is important to note that when we used a ball mill or mixer mill to conduct the machinery mechanical milling of 1-a and 1, the irreversible collapse of the network structure occurred, and we discovered Ag(0) particles in the PXRD patterns. All previous reports have stated that mechanically induced MOF/CP glass requires either a mixer mill or a ball mill, which is different from the case of 1. This probably means a major low elastic modulus of 1, and, therefore, the hand-grinding process is sufficient to produce its glassy state. Figs 3A and 3B show the XAS spectra of 1-MIG. The Ag *K*-edge XANES of 1-MIG is identical to that of 1-a and 1, illustrating that +1 oxidation state is maintained in 1-MIG. The Ag *K*-edge EXAFS spectrum of 1-MIG is same as that of 1, and the scattering pathways observed in RDFs for 1-MIG is similar to 1. It suggests that incident X-ray beams scattered by the neighboring atoms around Ag^+ with a same

fashion as like 1-a and 1. Considering that *p*L2 is a π-conjugated rigid structure, a slight distortion of coordination geometry in each Ag^{+}—which is hard to be detected by XAS studies—propagates the amorphization of the structure. To get more information on the structure of 1-MIG, X-ray total scattering structure functions ($S(Q)$) and its derived pair distribution functions ($G(r)$) for 1 and 1-MIG were collected (Fig. 4).[38] We discovered correlations even above 7 Å in 1-MIG, and this is partly because of the contribution of rigid and large *p*L2. Meanwhile, intense peaks at 2.2–2.4 Å would involve the radial distribution of Ag–O and Ag–N coordination bonds. These peaks in 1-MIG and coordination bonds were preserved as we studied XAS. Peaks at higher regions than 3.5–8 Å were also the same between 1 and 1-MIG.

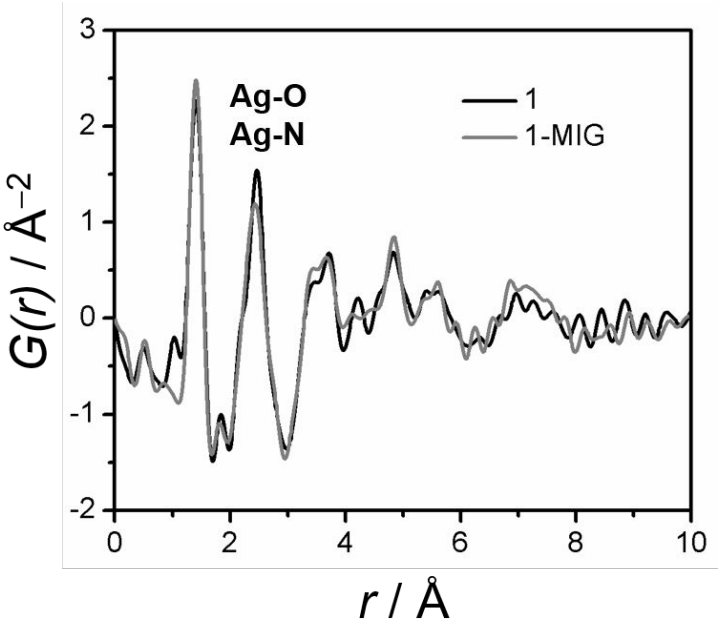

Fig. 4. Pair distribution function analysis of 1 and 1-MIG at room temperature.

TGA of 1-MIG (Fig. 5A) shows no weight loss up to 280 °C, which means that the mechanically induced amorphous state is thermally stable. The first heating cycle of DSC measurement of 1-MIG (Fig. 5B) exhibits an endothermic peak at 107 °C, an exothermic peak at 117 °C, and two more events at 233 °C and 267 °C. Because these two high-temperature events are relevant to those of 1, we confirm that the peak at 107 °C is T_g and that the peak at 117 °C is crystallization from 1-MIG to 1. To ensure that the peak at 117 °C is crystallization, we measured PXRD for 1-MIG and

treated it at 130 °C for 1 h (Fig. 5C). The peaks were broad but matched 1, and the exothermic event at 117 °C was crystallization (T_c). The crystallization of the glassy state of MOFs/CPs has been reported in the previous literature.[5, 13] T_g was not observed after the melting of 1-MIG during the cooling process to room temperature in the first cycle. In the second cycle, no signature of T_g and T_m appeared in both heating and cooling processes.

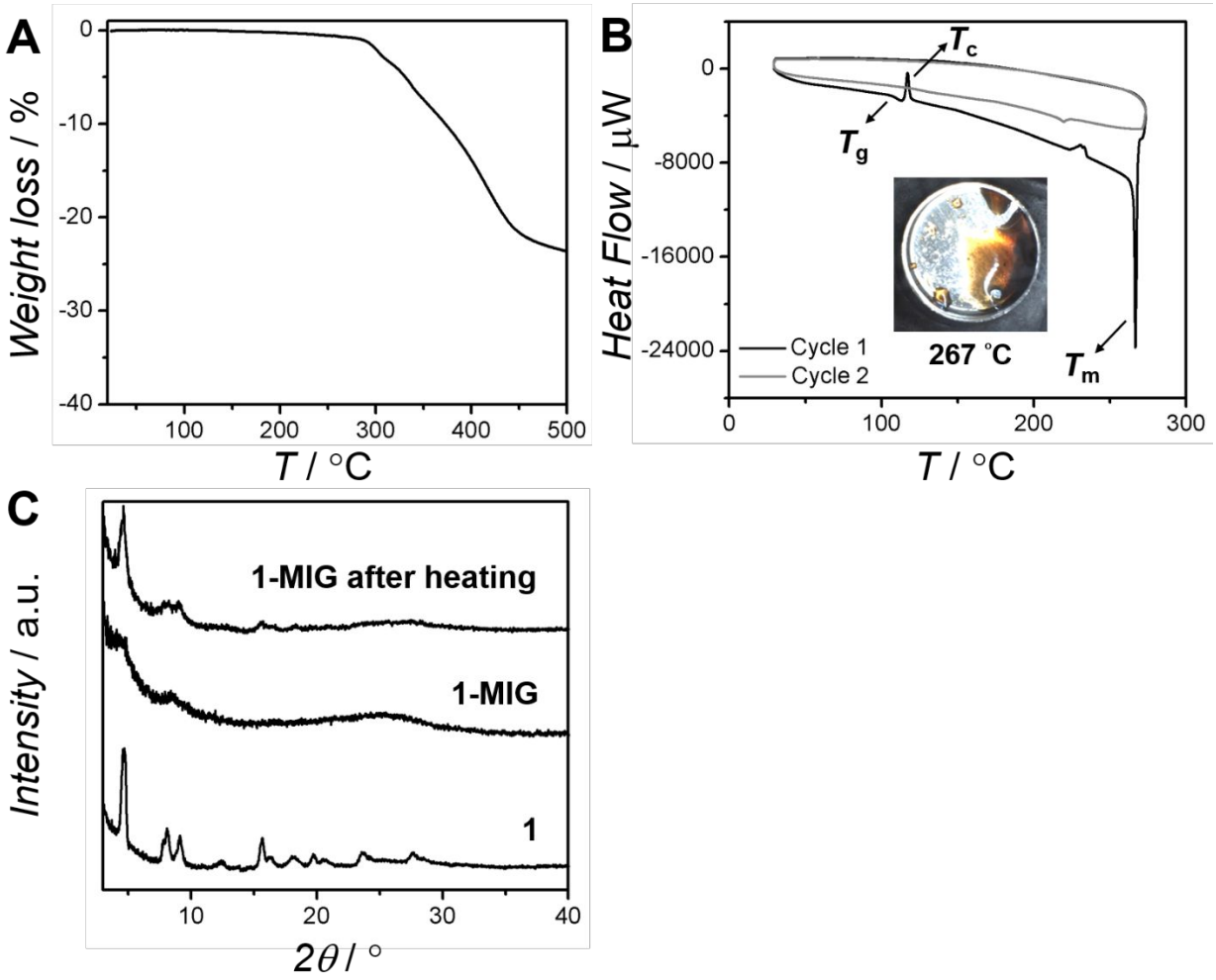

Fig. 5. (A) TGA profile of 1-MIG. The scan rate is 10 °C min^{-1}. (B) Two cycles of heating and cooling processes of DSC profiles of 1-MIG. *In situ* snapshots of 1 in the first heating process are also shown. T_m and T_c represent the melting and crystallization temperatures, and the ramping rate is 10 °C min^{-1}. (C) PXRD of 1-MIG heated at 130 °C for 1 h. For comparison, the patterns of 1 and 1-MIG are also shown.

Gas and vapor adsorption studies of 1 and 1-MIG

The glassy state of MOFs/CPs is limited, with fewer examples of those having gas adsorption properties.[6, 7] Exploring the porous MOF/CP glass is important for potential applications to the gas-permeable membrane and heterogeneous catalysis. To understand the porous nature of 1 and 1-MIG, we carried out CO_2 gas adsorption measurements at −78.15 °C (Fig. 6A). A gradual uptake of CO_2 was observed for 1 and 1-MIG, with increasing gas pressure and the total uptakes of both being low. At P_e = 103 kPa, the uptake amounts for 1 and 1-MIG were 4.8 and 9.2 mL g^{-1}, respectively. The desorption process of 1 and 1-MIG showed hysteresis, which means that the diffusion of CO_2 gases to both 1 and 1-MIG is low. This study indicates that 1 and 1-MIG retain some channels to incorporate CO_2 molecules and behave as porous compounds. We also carried out N_2 sorption isotherm measurements at −196.15 °C for both samples; neither of them showed any uptake.

To check the vapor affinity of solvents to 1 and 1-MIG, benzene vapor sorption measurements at 25 °C were carried out (Fig. 6B). The results indicated that 1 does not show any uptake of benzene from a pressure range of 0 to 12.3 kPa. However, 1-MIG showed a gate-opening type of adsorption behavior. It started an uptake of benzene vapor at 5.8 kPa, and the total amount of uptake reached 160 mL g^{-1} at P_e = 12.3 kPa. As we found in CO_2 isotherms, the desorption process showed broad hysteresis. This suggests that the interaction of framework and benzene solvent is strong in 1-MIG. By considering that the gate-opening type adsorption would be brought by structural change, we checked the structure of 1-MIG after the benzene sorption study. We retrieved the sample after the benzene sorption measurement and quickly measured PXRD (Fig. 6D). Although the observed peaks were broad, we found a glass-to-crystal transformation in the benzene sorption process. The peaks in the crystallized sample matched those of 1-a, which suggest that the benzene vapor induces crystallization and participates in the cavities to form 1-a. The H_2O vapor sorption measurement at 25 °C was also performed on 1 and 1-MIG (Fig. 6C). Both 1 and 1-MIG showed uptake in tandem with an increase in vapor pressure. At P_e = 3 kPa, 1 and 1-MIG had an uptake of water vapor with an amount of 104 and 128 mL g^{-1}, respectively. Through the desorption process, 1 and 1-MIG both released water with a small

hysteresis loop. We measured PXRD of 1-MIG after measuring H_2O vapor sorption (Fig. 6D). We found a few broad peaks at 2θ of 3.85° and 5°, with the overall structure being in an amorphous state. These broad peaks match those in 1, and we assume that the state of 1 after the H_2O sorption measurement was engaged in crystallization from 1-MIG to 1.

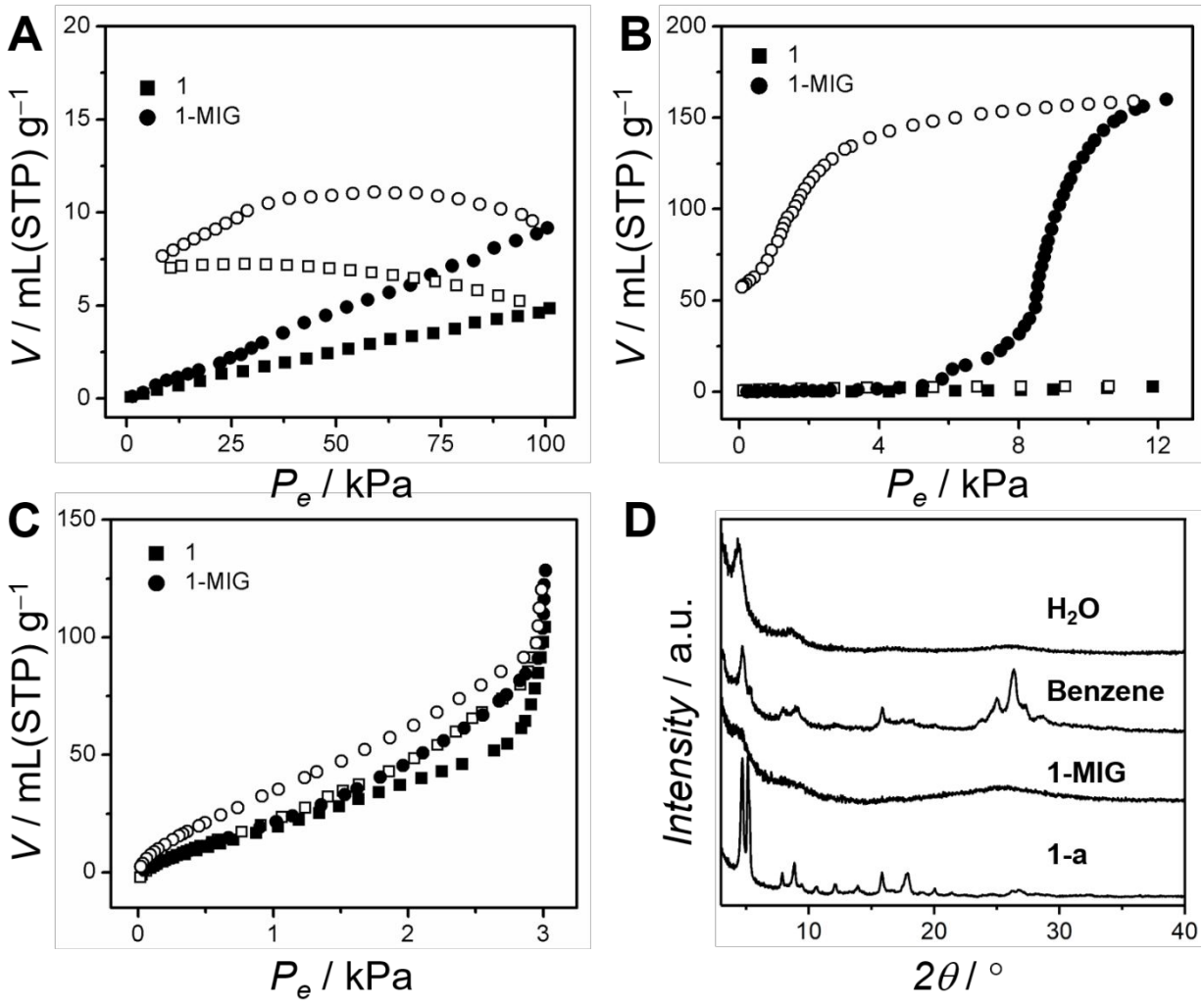

Fig. 6. (A) CO_2 adsorption study performed on 1 and 1-MIG at −78.15 °C. (B) Benzene vapor sorption measurement performed on 1 and 1-MIG at 25 °C. (C) Water vapor sorption measurement performed on 1 and 1-MIG at 25 °C. Black and white symbols represent adsorption and desorption, respectively. (D) PXRD of 1-MIG after the exposure of vapors of H_2O and benzene with the patterns of 1-MIG and 1-a.

Conclusions

To expand the library of melting MOFs/CPs, we selected 3D MOF $[Ag(pL_2)(CF_3SO_3)]\cdot 2C_6H_6$, composed of Ag^+ and tripodal nitrile ligand. We confirm that the guest-free structure retained the coordination network, and the state showed crystal melting at 271 °C; its glassy state was prepared by a gentle cooling of the liquid state. The fabrication of a glassy state was also observed by the mechanical grinding of the polycrystalline sample. The MOF glass maintained the coordination environment around Ag^+, which was confirmed by XAS, X-ray total scattering analyses, and FT-IR studies. The gas and vapor sorption studies have illustrated the permanent porosity of the glassy state and the ability of crystallization to the original 3D structure by vapor exposure. This work clarified that nitrile ligand-based MOFs belong to the family of crystal melting and vitrification behaviors. This research recommends identifying more examples of melting MOFs within nitrile groups.

Acknowledgement

The work was supported by the Japan Society of the Promotion of Science (JSPS) for a Grant-in-Aid for Scientific Research (B) (JP18H02032) and Challenging Research (Exploratory) (JP19K22200) from the Ministry of Education, Culture, Sports, Science and Technology, Japan, and Strategic International Collaborative Research Program (SICORP) and Adaptable and Seamless Technology Transfer Program through Target-driven R&D (A-STEP) from the Japan Science and Technology, Japan.

References

1. D. Umeyama, S. Horike, M. Inukai, T. Itakura and S. Kitagawa, *J. Am. Chem. Soc.*, 2015, **137**, 864.
2. T. D. Bennett, J. C. Tan, Y. Yue, E. Baxter, C. Ducati, N. J. Terrill, H. H. Yeung, Z. Zhou, W. Chen, S. Henke, A. K. Cheetham and G. N. Greaves, *Nat. Commun.*, 2015, **6**, 8079.

3. T. D. Bennett and S. Horike, *Nat. Rev. Mater.*, 2018, **3**, 431.
4. S. Horike, S. S. Nagarkar, T. Ogawa and S. Kitagawa, *Angew. Chem., Int. Ed.*, 2019, DOI: 10.1002/anie.201911384
5. W. Chen, S. Horike, D. Umeyama, N. Ogiwara, T. Itakura, C. Tassel, Y. Goto, H. Kageyama and S. Kitagawa, *Angew. Chem. Int. Ed.*, 2016, **55**, 5195.
6. M. Inukai, Y. Nishiyama, K. Honjo, C. Das, S. Kitagawa and S. Horike, *Chem. Commun.*, 2019, **55**, 8528.
7. C. Zhou, L. Longley, A. Krajnc, G. J. Smales, A. Qiao, I. Erucar, C. M. Doherty, A. W. Thornton, A. J. Hill, C. W. Ashling, O. T. Qazvini, S. J. Lee, P. A. Chater, N. J. Terrill, A. J. Smith, Y. Yue, G. Mali, D. A. Keen, S. G. Telfer and T. D. Bennett, *Nat. Commun.*, 2018, **9**, 5042.
8. L. Frentzel-Beyme, M. Kloss, P. Kolodzeiski, R. Pallach and S. Henke, *J. Am. Chem. Soc.*, 2019, **141**, 12362.
9. A. Qiao, T. D. Bennett, H. Tao, A. Krajnc, G. Mali, C. M. Doherty, A. W. Thornton, J. C. Mauro, G. N. Greaves and Y. Yue, *Sci. Adv.*, 2018, **4**, 1.
10. A. Qiao, H. Tao, M. P. Carson, S. W. Aldrich, L. M. Thirion, T. D. Bennett, J. C. Mauro and Y. Yue, *Opt. Lett.*, 2019, **44**, 1623.
11. T. D. Bennett, Y. Yue, P. Li, A. Qiao, H. Tao, N. G. Greaves, T. Richards, G. I. Lampronti, S. A. Redfern, F. Blanc, O. K. Farha, J. T. Hupp, A. K. Cheetham and D. A. Keen, *J. Am. Chem. Soc.*, 2016, **138**, 3484.
12. S. Horike, D. Umeyama, M. Inukai, T. Itakura and S. Kitagawa, *J. Am. Chem. Soc.*, 2012, **134**, 7612.
13. Y. Ohara, A. Hinokimoto, W. Chen, T. Kitao, Y. Nishiyama, Y. L. Hong, S. Kitagawa and S. Horike, *Chem. Commun.*, 2018, **54**, 6859.
14. S. S. Chui, S. M. Lo, J. P. Charmant, A. G. Orpen and I. D. Williams, *Science*, 1999, **283**, 1148.
15. M. Eddaoudi, J. Kim, N. Rosi, D. Vodak, J. Wachter, M. O'Keeffe and O. M. Yaghi, *Science*, 2002, **295**, 469.
16. J. H. Cavka, S. Jakobsen, U. Olsbye, N. Guillou, C. Lamberti, S. Bordiga and K. P. Lillerud, *J. Am. Chem. Soc.*, 2008, **130**, 13850.

17. J. M. Taylor, R. K. Mah, I. L. Moudrakovski, C. I. Ratcliffe, R. Vaidhyanathan and G. K. Shimizu, *J. Am. Chem. Soc.*, 2010, **132**, 14055.
18. D. Sheberla, L. Sun, M. A. Blood-Forsythe, S. Er, C. R. Wade, C. K. Brozek, A. Aspuru-Guzik and M. Dincă, *J. Am. Chem. Soc.*, 2014, **136**, 8859.
19. L. E. Darago, M. L. Aubrey, C. J. Yu, M. I. Gonzalez and J. R. Long, *J. Am. Chem. Soc.*, 2015, **137**, 15703.
20. J. F. Keggin and F. D. Miles, *Nature*, 1936, **137**, 577.
21. K. A. Hofmann and F. Küspert, *Z. Anorg. Allg. Chem.*, 1897, **15**, 204.
22. B. F. Hoskins and R. Robson, *J. Am. Chem. Soc.*, 1989, **111**, 5962.
23. A. L. Goodwin, K. W. Chapman and C. J. Kepert, *J. Am. Chem. Soc.*, 2005, **127**, 17980.
24. W. Kaneko, M. Ohba and S. Kitagawa, *J. Am. Chem. Soc.*, 2007, **129**, 13706.
25. N. Lock, Y. Wu, M. Christensen, L. J. Cameron, V. K. Peterson, A. J. Bridgeman, C. J. Kepert and B. B. Iversen, *J. Phys. Chem. C*, 2010, **114**, 16181.
26. E. Coronado and G. Minguez Espallargas, *Chem. Soc. Rev.*, 2013, **42**, 1525.
27. Z. Liu, Q. Gao, J. Chen, J. Deng, K. Lin and X. Xing, *Chem. Commun.*, 2018, **54**, 5164.
28. G. B. Gardner, D. Venkataraman, J. S. Moore and S. Lee, *Nature*, 1995, **374**, 792.
29. E. Lorch, *J. Phys. C: Solid State Phys.*, 1969, **2**, 229.
30. B. Ravel and M. Newville, *J. Synchrotron Radiat.*, 2005, **12**, 537.
31. T. Ueda, T. Tominaga, T. Mochida, K. Takahashi and S. Kimura, *Chem. Eur. J.*, 2018, **24**, 9490.
32. Y. Funasako, S. Mori and T. Mochida, *Chem. Commun.*, 2016, **52**, 6277.
33. A. Bianconi, *Appl. Surface Sci.*, 1980, **6**, 392.
34. D. Norman, *J. Phys. C: Solid State Phys.*, 1986, **19**, 3273.
35. Y. Yin, W. Xu, Z. Tan, Y. Li, W. Wang, X. Guo, S. Yu, J. Liu and G. Jiang, *Environ. Pollut.*, 2017, **220**, 955.
36. A. Hayashi, T. Ohtomo, F. Mizuno, K. Tadanaga and M. Tatsumisago, *Electrochem. Commun.*, 2003, **5**, 701.
37. J. F. Willart and M. Descamps, *Mol. Pherm.*, 2008, **5**, 905.
38. R. E. Whitfield, D. J. Goossens and T. R. Welberry, *IUCrJ*, 2016, **3**, 20.